Materials and Design 31 (2010) 4943–4950

Contents lists available at ScienceDirect

Materials and Design

journal homepage: www.elsevier.com/locate/matdes

Technical Report

Fracture toughness (J_{1C}) of electron beam welded AA2219 alloy

Biju S. Nair [a,*], S. Rakesh [a], G. Phanikumar [b], K. Prasad Rao [b], P.P. Sinha [a]

[a] Vikram Sarabhai Space Center, Thiruvananthapuram, Kerala 695 022, India
[b] Department of Metallurgical and Materials Engineering, Indian Institute of Technology Madras, Chennai 600 036, India

ARTICLE INFO

Article history:
Received 4 March 2010
Accepted 8 May 2010
Available online 13 May 2010

ABSTRACT

AA2219 (Al–6%Cu) was butt welded in T87 temper (solution heat-treated, cold worked and precipitation hardened) and T6 temper (solution heat-treated and precipitation hardened) using electron beam welding (EBW). Variables studied were base metal temper condition and mode of EBW. Mechanical properties of the weld joint and fracture toughness at fusion zone (FZ) and heat-affected zone (HAZ) were evaluated and compared with those of the base metal. Results showed that EB welds have higher joint efficiency and fracture toughness than that of gas tungsten arc welding (GTAW). Fracture toughness of T6 base metal was found to be higher than its T87 counterpart. When welded, FZ and HAZ in T87 showed higher fracture toughness than that of T6; HAZ was the toughest. Pulsed current (PC) EB weld showed marginal reduction in toughness compared to constant current (CC) weld. Toughness variation is analyzed with the help of tensile test, Charpy impact test and scanning electron microscopy (SEM) and transmission electron microscopy (TEM).

1. Introduction

Vessels made out of AA2219 (Table 1 shows the chemical composition) are used for storing liquid oxygen (−183 °C/90 K), liquid hydrogen (−253 °C/20 K) and other liquid engine fuels for aerospace application. This is due to its dependable mechanical properties and fracture toughness over wide range of temperatures.

Alloy composition of AA2219 is less sensitive to solidification cracking [1]. Its weld joint efficiency is found to depend on base metal temper. Joint efficiency close to 100% can be achieved when base metal is in annealed state [2], which could be due to near matching of cast structures.

AA2219 alloy is normally used in T87 temper for high specific strength. However, due to solute segregation and dissolution of strengthening precipitates during welding, the weld efficiency drops considerably. GTAW with arc manipulation techniques [3], addition of scandium filler [4,5] and multipass in direct current electrode negative (DCEN) polarity [6] were shown as a few ways to improve the mechanical properties of weld joint. Earlier works showed that EBW increases weld strength of AA2219 alloy [7] and further improvement was reported with EBW in PC mode [6]. Predominant factors that influence its joint strength are grain refinement, copper segregation, partially melted zone (PMZ) and precipitate free regions. In EBW, the solidification rate is very high. This is responsible for high dislocation density, fine-grained microstructure and low solute segregation. From the point of view of strength, the effect of low solute segregation is to enhance solute diffusion into the aluminium rich α phase and consequently solid solution hardening. High solute saturation favors natural aging reaction and subsequent precipitation hardening.

Results of crack propagation study in the FZ and HAZ (plasma arc welding) of 7 mm AA2219-T851 are described in Ref. [8]. Fine tensile voiding, grain boundary failure, intergranular shear and coarse voiding at large intermetallics were attributed to the fracture of aluminium alloys 7449 and 7150 [9]. Fracture toughness of high strength aluminium alloys is known to be influenced by base metal temper, yield strength, dispersoid and intermetallic contents, slip behavior, grain and grain boundary structure [10]. Two thousand series aluminium alloys generally exhibit lower fracture toughness in under-aged state compared to peak-aged condition. Studies carried out on AA2219 showed that strength–toughness relation follows a conventional inverse relation up to peak-aged state. Narayana et al. [11] studied fracture behavior of 7 mm thick AA2219-T87 GTAW plates. Their study showed average fracture toughness (J_{1C}) of 33.4 kJ/m^2 at the HAZ, 21 kJ/m^2 at the FZ and 16.6 kJ/m^2 at the PMZ. Unlike GTAW, EBW is an energy intensive welding process. Microstructural responses are far different in these two cases. Although, previous studies established advantages of EBW for AA2219, fracture toughness of these welds was not analyzed. In this paper, J_{1C} analysis of 7 mm thick EBW plates in CC and PC welding modes and two base metal tempers is presented. Since PMZ is insignificant in EBW, two zones viz. FZ and HAZ were studied. Mechanical properties such as tensile and Charpy toughness of these welds were also evaluated and related with their microstructural features.

* Corresponding author. Tel.: +91 4712562474; fax: +91 4712705427.
E-mail address: s_biju@vssc.gov.in (B.S. Nair).

0261-3069/$ - see front matter © 2010 Elsevier Ltd. All rights reserved.
doi:10.1016/j.matdes.2010.05.017

Table 1
Chemical composition (wt.%) of AA2219 alloy.

Cu	Mn	Zr	V	Ti	Fe	Si	Al
5.95	0.27	0.10	0.09	0.06	0.10	0.05	Bal

2. Experimentation

An electron beam welding machine of 60 kV, 500 mA power rating was used for welding experiments. AA2219 plates in T87 temper and T6 temper of 7.0 mm thickness, 60 mm wide and 250 mm long were welded along the length. All experiments were carried out at a fixed work distance of 260 mm from the bottom face of electron gun. Pulsing was achieved by switching the beam current on and off at 66.6 Hz frequency. On and off durations were optimized for 7.5 ms each. EB welds in CC and PC modes were made with approximate heat input of 170 J/mm and 150 J/mm respectively.

Optical microscope (OM) and SEM were used for microstructural observation. Energy dispersive X-ray analysis (SEM EDAX) was used for microanalysis of solute content (copper) across the grains. TEM was used to observe the absence or presence of strengthening precipitates and TEM EDAX was used for precipitate analysis. Micro hardness survey was carried out with 100 g load. Transverse tensile test was performed as per ASTM E 8 M standard. Impact strength was measured using sub-size Charpy V-notch samples as per ASTM E-23 standard.

Compact tension specimens for J_{1C} analysis (Fig. 1a) were made as per ASTM E-813 standard [12]. Width to thickness ratio of four has been maintained in all the specimens. Starter notch was made parallel to the welding direction at two locations (center of FZ and HAZ) in welded specimens as shown in Fig. 2 and perpendicular to rolling direction in BM. As shown in Fig. 2, the FZ was typically broad at the top layer (4 mm). Sudden change to narrow and near uniform FZ is also typical for full penetration EBW with sufficient power density. In this work, neglecting the crown area, FZ width was measured to be 1.2 mm. For analyzing the fracture toughness at the HAZ, notch tip was machined at 1.8 mm from the fusion line ('a' in Fig. 2). Similarly, center of the notch in the FZ ('b' in Fig. 2) was made at 0.6 mm from the fusion line. Grooving along uncracked ligament ensured straight crack growth. Single specimen evaluation technique was employed. Fatigue pre-cracking was done in tension–tension mode in a servo hydraulic testing apparatus at 20 Hz and stress ratio 0.1. Pre-cracking was continued in three steps (machined notch length 12.8–13.3 mm, 13.3 – 13.8 mm and 13.8–14.3 mm at a maximum load of 1.1 kN, 0.9 kN and 0.8 kN respectively) at controlled laboratory environment. Monotonic loading for incremental crack growth continued for each programmed load-line displacement. This was followed by

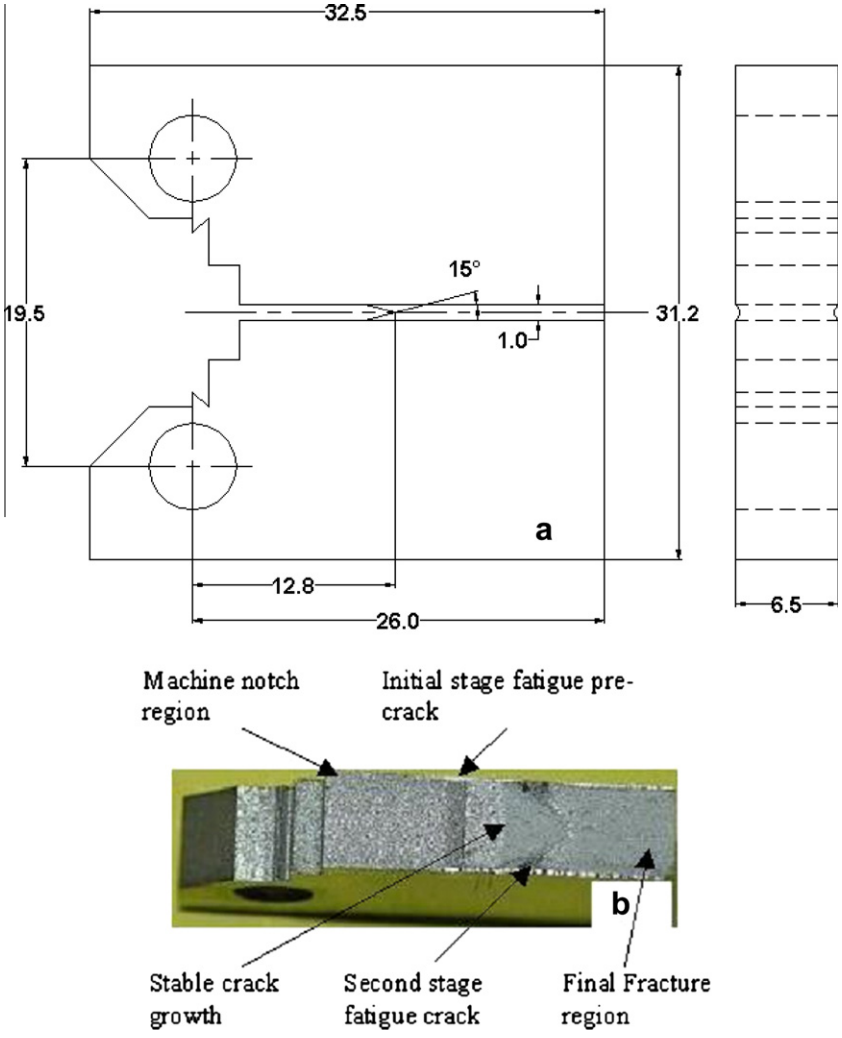

Fig. 1. (a) J_{1C} (fracture toughness) test specimen (ASTM E1820) and (b) typical fracture surface after test.

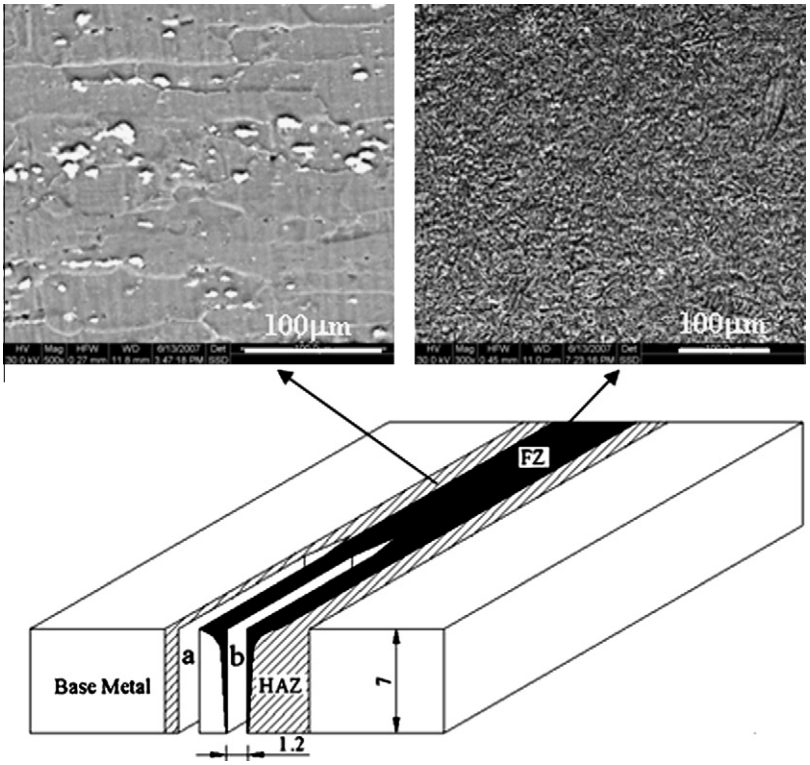

Fig. 2. Schematic depicting crack tip locations in the fusion zone and heat-affected zone and the corresponding SEM images.

secondary fatigue cracking and loading till failure. Three specimens were tested to arrive at an average value for each category. A typical fracture surface of the tested specimen is shown in Fig. 1b.

3. Results and discussion

3.1. Microstructure

Microstructure of AA2219 consists of α phase, eutectics and θ phase. Shape and size of grains, size and distribution of second phase, size and orientation of strengthening precipitates and dislocation density are different in T87 temper and T6 temper. This change is due to heat-treatment process variation. EBW was carried out to join these base metals with power density above 10^7 W/cm^2. Compared with single pass GTAW, for full penetration butt welding, quantity of heat needed in EBW was less by an order. Major welding process parameters and its influence on solidification are given in Table 2. It can be noticed that as the heat input lowered, the cooling rate increased and the solidification became faster.

Fig. 3 shows micrographs at the FZ of EBW in T87 base metal. Sub-grain solidification in the FZ was found to be cellular. Intercellular eutectic phase was thin and discontinuous. This is in line with the observation that if the weld solidification rates are quite rapid, full dendrites may not develop and shorter projections called cell structure would form [13]. Microanalysis showed that eutectic phases correspond to hypoeutectic of Al–Cu. Its size and volume fraction in the FZ of PC weld (Fig. 3b) was found to be smaller than CC (Fig. 3a) counter part. TEM analysis (Fig. 4) within the FZ showed dislocations whose density in PC weld was observed to be far above the CC weld (Fig. 4b). In T6 base metal, because of large prior θ phase [14], size of eutectic phase in the FZ was proportionately large.

3.2. Mechanical properties

3.2.1. Hardness

Micro hardness measurements were taken along the weld cross-section at 3.5 mm distance from top of weld bead. Hardness plot (Fig. 5) is indicative of size of HAZ and FZ. Decrease in hardness at the HAZ was the result of dissolution of strengthening precipitates near interface and over aging towards unaffected base metal. Because of reduction in heat input and additional cooling effect, cross-section of PC weld was relatively narrow. FZ hardness of PC weld was found approximately 10HV higher than CC weld.

3.2.2. Tensile properties

Results of room temperature transverse tensile testing are given in Table 3. Three specimens were tested and average value is reported. For an assessment of weld joint efficiency, BM strength is given. BM in T6 temper has low precipitate density, which was the reason for its high ductility over T87 counterpart. Tensile failures of the welds were along the fusion boundary.

Table 2
Welding parameters – welding current (I), acceleration voltage (V), travel speed (v) and computed values of cooling rate (R) and solidification time (S_t).

Welding type	Mode	I (Amp)	V (Volt)	v (mm/s)	H_{net} (J/mm)	R (K/s)	S_t (s)
EBW	CC	95×10^{-3}	60×10^3	30	171	780	0.23
EBW	PC	125×10^{-3}	60×10^3	23	147	1106	0.21
GTAW*	CC	300	18	3	1620	9.1	2.37

* Single pass, direct current, electrode negative.

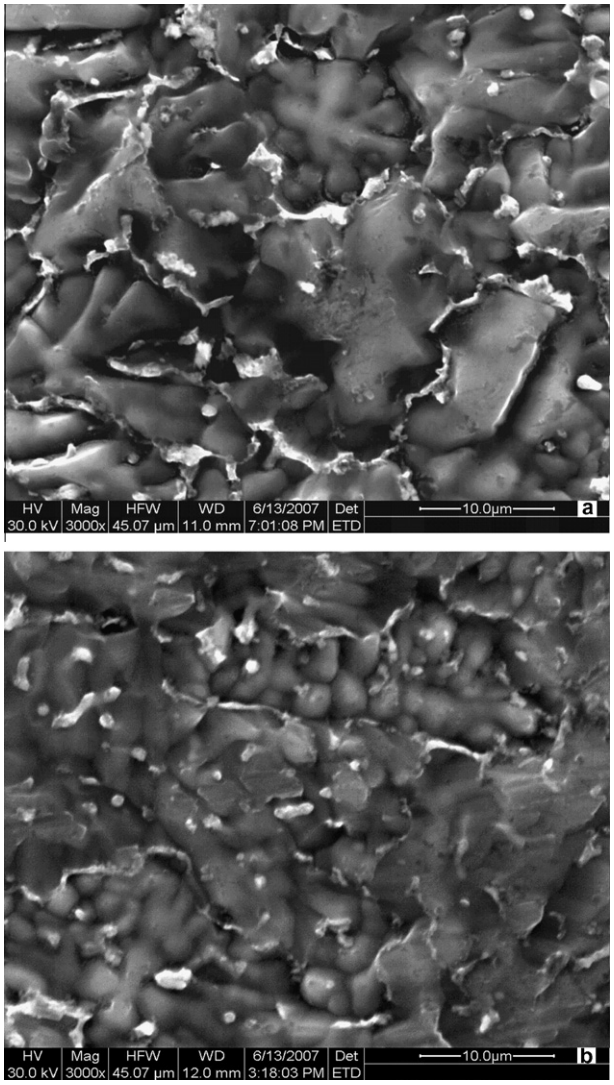

Fig. 3. SEM imaging of fusion zone microstructure; (a) EBW in constant current mode (b) EBW in pulsed current mode.

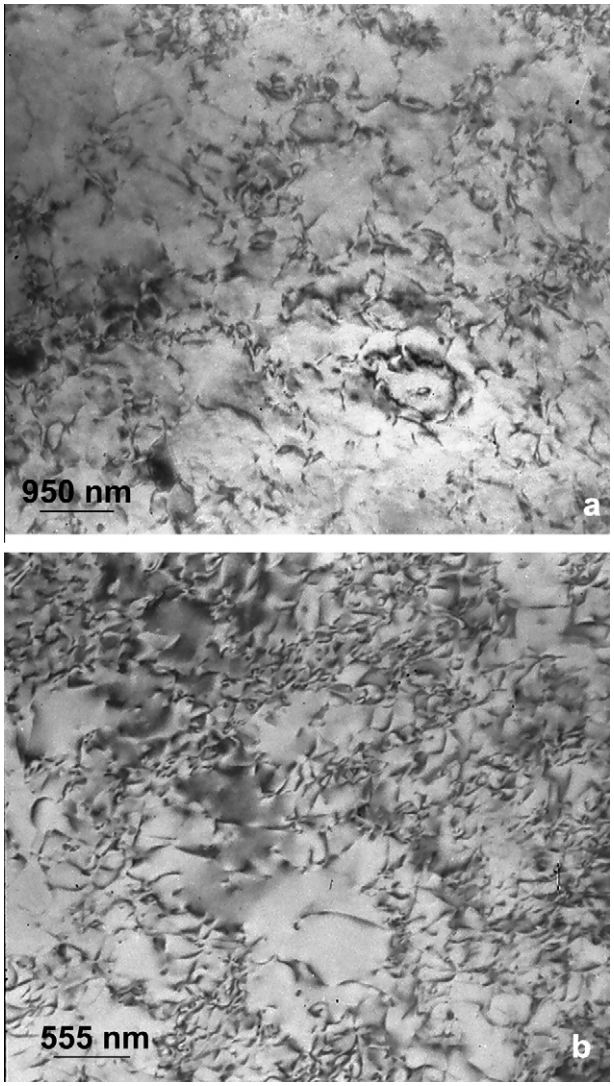

Fig. 4. TEM imaging of fusion zone microstructure; (a) EBW in constant current mode (b) EBW in pulsed current mode.

3.2.3. Impact toughness

Table 4 shows results of impact toughness evaluation. Compared to base metal in T6 and T87 tempers, respective EBW specimens showed higher impact toughness values (beyond 200%), which verified the ductility and high strain rate loading capability of EB welds. As shown in Table 3, ductility of T6 base metal was higher than T87 base metal and retained similar trends when welded. Amongst both temper states, T6 exhibited superior impact toughness.

3.2.4. Fracture toughness

Fig. 6 shows experimentally determined fracture toughness (J_Q) curves pertaining to T87 base metal and Fig. 7 shows similar curves of T6 base metal. J_Q corresponds to intersection of best fitted curves through J points and exclusion line drawn parallel to the blunting line (blunting point = $(\sigma_y + \sigma_u)\triangle a$) with 0.2 mm incremental crack extension. J_Q was verified for J_{1C} according to the following validity criterions:

(1) Specimen thickness $B > 25J_Q/\sigma_y$
(2) Initial ligament $(w–a_0) > 25J_Q/\sigma_y$.

For convenience, graphs depicted in Figs. 6 and 7 were plotted with blunting point computed based on base metal properties. Actual values given in Tables 5 and 6 were computed with σ_y and σ_u obtained from respective tension tests (Table 3).

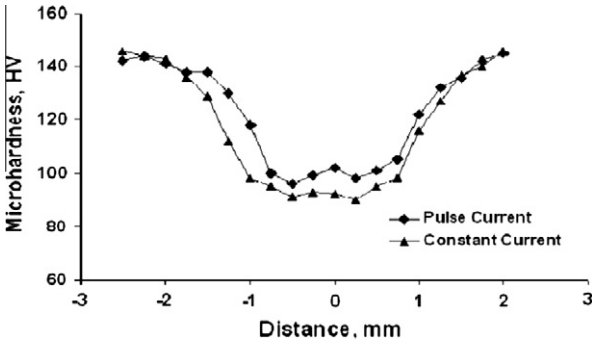

Fig. 5. Microhardness measurement along fusion zone of EBW in T87 base metal (mapped from center of weld to unaffected base metal).

3.2.4.1. Base metal. It was found that depending on initial temper condition fracture toughness of AA2219 alloy varies. In this work, experimentally validated J_{1C} values were 9.3 kJ/m^2 in T87 and

Table 3
Tensile strength of electron beam welds; CC – constant current, PC – pulsed current, BM – base metal.

Type of sample	UTS (MPa)	0.2% YS (MPa)	El% (25 mm GL)
CC (T87)	301	196	4.6
PC (T87)	317	211	4.8
BM (T87)	464	366	9.0
CC (T6)	321	189	7.6
PC (T6)	313	178	7.2
BM (T6)	453	325	15.0

Table 4
Impact energy of electron beam welds, CC – constant current, PC – pulsed current, BM – base metal in T6 and T87.

Type of sample	Impact energy (Nm)
CC (T87)	8.1
PC (T87)	8.8
BM (T87)	3.9
CC (T6)	10.1
PC (T6)	10.7
BM (T6)	5.1

Table 5
Experimentally determined fracture toughness (J_Q) at FZ of EBW. σ_y – cross-transverse yield strength of EBW in constant current and pulsed current modes, w – width of test specimen, a_0 – length of ligament beyond machined crack.

Base metal	Mode	J_Q (kJ/m^2)	$25J_Q/\sigma_y$	w–a_0 (mm)
T87	CC	35.8	3.59	11.84
	PC	29.8	2.99	12.28
T6	CC	37.46	3.80	11.87
	PC	37.36	3.66	11.70

Table 6
Experimentally determined fracture toughness (J_Q) at HAZ of EBW. σ_y – cross-transverse yield strength of EBW in constant current and pulsed current modes, w – width of test specimen and a_0 – length of ligament beyond machined crack.

Base metal	Mode	J_Q (kJ/m^2)	$25J_Q/\sigma_y$	w–a_0 (mm)
T87	CC	54.4	3.59	11.84
	PC	29.8	2.99	12.28
T6	CC	37.46	3.80	11.87
	PC	40.24	3.66	11.70

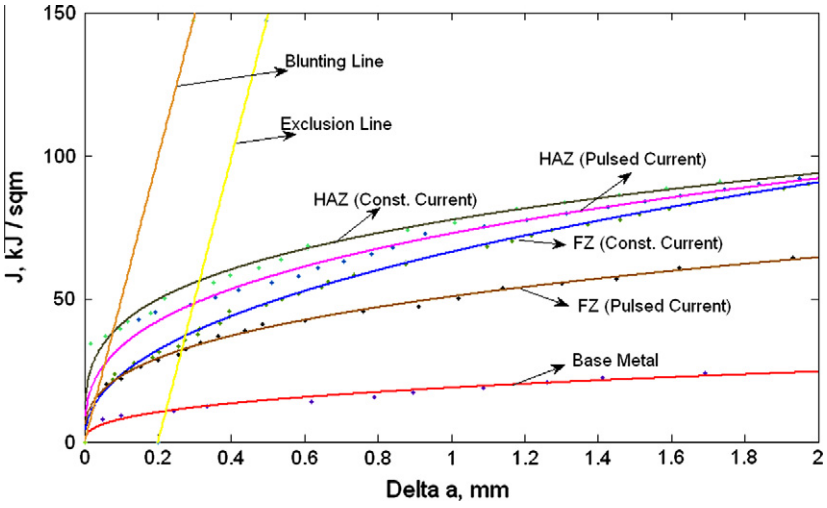

Fig. 6. Measurement of experimental fracture toughness (J_Q) – base metal in T87 temper.

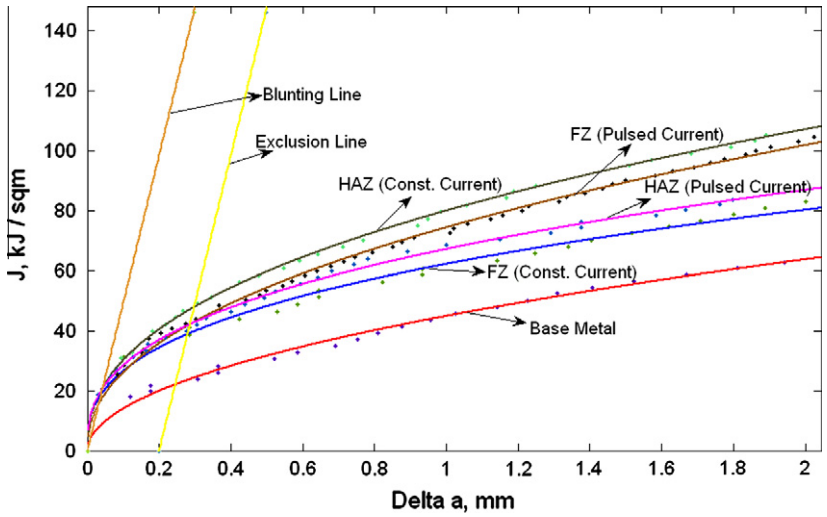

Fig. 7. Measurement of experimental fracture toughness (J_Q) – base metal in T6 temper.

18.19 kJ/m^2 in T6. This distinction is in agreement with the ductility obtained in uniaxial tension test (Table 3) and energy absorbed in Charpy test (Table 4).

Precipitation of fine needle shaped $CuAl_2$ is the principal strengthening mechanism of AA2219. Low fracture toughness of base metal in T87 temper can be attributed to the ductile tearing in the matrix at zones of these precipitate. During loading for fracture toughness test, stress at crack tip will be much higher than the yield stress. Small and coarse precipitates appearing in the strain field shall nucleate voids. Fine precipitates have least inter-particle spacing. When voids are formed at these zones, ligaments between voids reduce and lead to void coalescence. This way fine precipitates in the base metal assist merger of voids with crack front and take part in ductile tearing without expending much energy [15]. Major difference between heat-treatment tempers T87 and T6 is quantity, size and orientation of strengthening precipitates. Large number of fine plate like precipitates in T87 temper explains the major reason for high strength, low ductility and low fracture toughness of T87 base metal.

3.2.4.2. Electron beam weld. Comparing with GTAW (Fig. 8a), the microstructure of EBW (Fig. 8b) was highly refined. Sub-structure solidification was cellular and segregation was the least (Fig. 3). As-weld FZ was enriched with dislocations but free of strengthening precipitates (Fig. 4). Melted volume and heat-affected volume were highly limited. PMZ was almost absent. FZ and HAZ being significant, for fracture toughness analysis these zones were chosen.

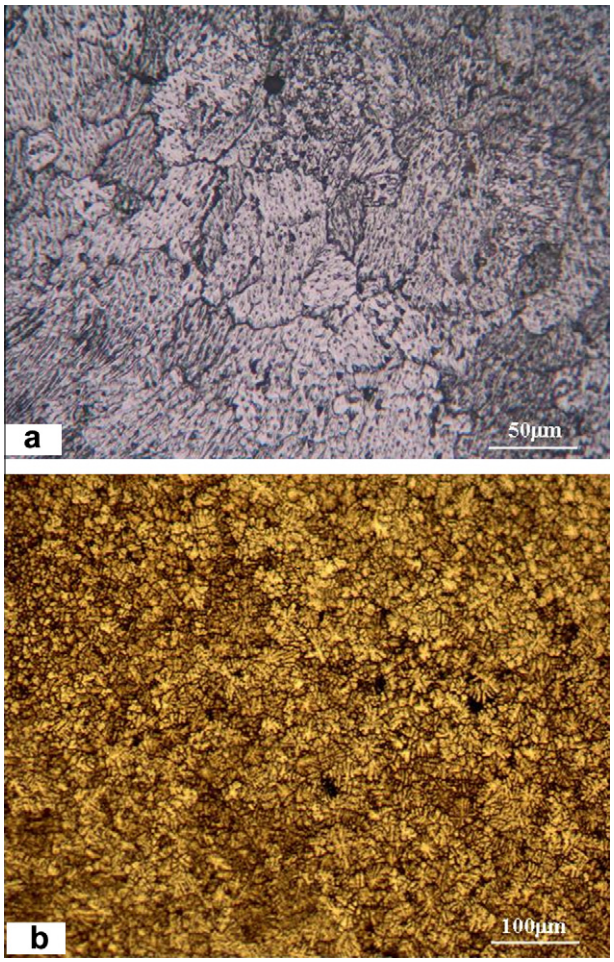

Fig. 8. Optical microstructure at the fusion zone; (a) single pass gas tungsten arc weld (b) electron beam weld.

3.2.4.2.1. Fusion zone. Starter notch was made along the weld length through the center of the FZ. Crack tip location and corresponding microstructure are shown in Fig. 2. Similar to the impact toughness, J_{1C} analysis showed higher values than the corresponding base metal. CC weld demonstrated higher fracture toughness than PC weld (Table 5). Similarly, weld in T6 temper was tougher than that in T87 temper. Reasons for these findings are given as follows:

Because of focused electron beam and faster processing rate, FZ of EBW has the benefit of fine-grained microstructure. Grain size, sub-grain microstructure, solute partitioning, eutectic network and strengthening precipitates were the major factors that influenced FZ fracture resistance. Fine grains favored ductility and fracture resistance because grain boundary is a strong barrier for propagation of micro cracks [16].

Compared with GTAW, eutectic distribution around cell boundary in the FZ of EBW (Fig. 3) was weak and discontinuous. Cu-rich areas were found at inter cellular spaces, which were analyzed using SEM EDAX and found to be $CuAl_2$ intermetallic. Al-rich phase being ductile, propagation of crack through these fine cellular structure would be delayed due to plastic zone formation ahead of crack tip and expend a lot of energy before onset of stable crack growth. Because of near solution heat treatment attained from heat of welding, FZ of EBW was almost free of strengthening precipitates (Fig. 4), which enhanced FZ fracture toughness. Crack propagation through FZ could be by void nucleation at Cu-rich area, void growth, crack jumping and blunting at cellular matrix.

T87 Temper: This temper was achieved by cold rolling after solution heat-treatment and then precipitation hardening. Cold working was meant to create dislocations, which enabled heterogeneous nucleation of strengthening precipitates at dislocation sites. Solidification time in EBW process was estimated to be around 0.2 s. This implies significantly higher quenching rate in the FZ and insufficient welding time for complete annihilation of prior dislocations. TEM micrographs at the FZ of EBW showed dislocations (Fig. 4). Its severity could be a reason for void nucleation and de-bonding. It was also found that dislocation density in the FZ of PC weld (Fig. 4b) was more than that in CC weld (Fig. 4a). Higher quench rate in PC welds was the reason for this increase. Correspondingly PC welds showed marginal reduction in fracture toughness.

T6 Temper: BM in T6 temper state was ductile than T87 temper (Table 3). Significant differences to be considered among EBW in these tempers are: (1) size of undissolved θ phase (2) quantity, size and distribution of eutectics in FZ (3) dislocation density in the as-weld matrix. Due to melting and solidification in fusion welding, it was likely that properties at FZ of T6 temper may match with T87 temper. However, with EBW, it was found that tensile strength, tensile elongation and impact resistance varied between these two tempers (Tables 3 and 4). Fracture toughness evaluation with crack along centerline of FZ showed marginal rise of fracture toughness in T6 temper compared to similar work in T87 weld. Among T6 temper, fracture toughness of CC and PC modes were nearly the same.

Higher fracture toughness at the FZ of T6 temper could be due to its prior thermal condition which is free from dislocations. As discussed earlier, T87 BM is enriched with dislocations. Annihilation of such defects might not be complete in a faster welding process like EBW, where a focused beam was made to traverse at a velocity of 30 mm/s. Role of prior dislocations in controlling the fracture toughness between two base metal tempers could be verified using the estimated cooling rates (Table 2). From 780 K/s, the cooling rate increased to 1100 K/s in PC weld. However, in the case of FZ fracture toughness of welds in T6 base metal, the effect of this variation in cooling rates was not observed between CC and PC modes (Table 5). This verified the role of dislocations in regulating the fracture toughness at FZ.

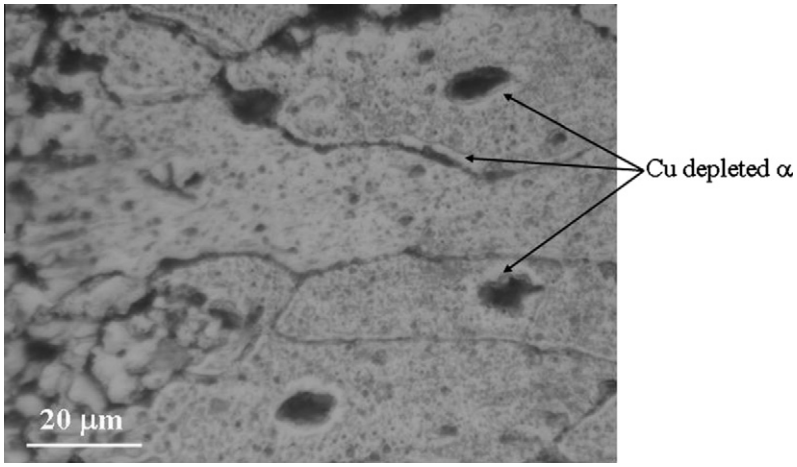

Fig. 9. Optical micrograph showing microstructure at heat-affected zone.

3.2.4.2.2. Heat-affected zone. Starter notch was made along the weld length at 2.4 mm offset from the center of FZ. Crack tip location and corresponding microstructure are shown in Fig. 2. Highest fracture toughness was found at HAZ. In this case also CC welds were found to be tougher than PC welds (Table 6).

HAZ contained undissolved coarse constituent $CuAl_2$ particles and sparsely populated incoherent equilibrium θ precipitates, which were surrounded by soft Cu depleted matrix of aluminium rich α phase. Copper depleted α solidification appeared as light etched phase along grain boundary eutectics and as light etched rings surrounding isolated θ particles [14,17]. With less solute in α phase, lesser would be the solution strengthening effect, which reduced strength and increased ductility at such zones. It was shown in the work of Narayana et al. [11] that due to heat of welding, there was complete reversion of strengthening precipitates at zones closer to the FZ of GTAW, where temperature was beyond that of solvus and time was inadequate for re-precipitation [11]. Unlike BM, at HAZ a lot of energy was expended in the formation of voids. This was because copper depleted α zones around θ particles resisted crack growth by plastic deformation. Although width of HAZ in EBW was lesser than GTAW, the temperature involved in the zones very close to FZ was beyond that of solvus of metastable phases and this time–temperature reaction was likely to cause dissolution/reversion of strengthening precipitates. In either case, this region had enhanced ductility and fracture toughness. Inter-particle distance increased due to precipitate dissolution. Comparing to FZ comprising fine-grained microstructure and weak intercellular brittle phase, at HAZ grain size was very large. In this zone, void nucleation has to be mainly at particle–matrix interface. However, void nucleation was delayed due to scarcely populated precipitates and its merger was postponed due to copper depleted ductile matrix surrounding the second phase (Fig. 9).

T87 Temper: It was found that fracture toughness at HAZ of T87 CC EBWs was the highest (Table 6). Reasons for this increase are mainly due to: (1) dissolution of strengthening precipitates (2) lesser volume fraction of second phase in T87 than that in T6 temper. Reduction in fracture toughness at HAZ with current pulsing could be attributed to its low heat input and high cooling rate, which reduced both width of heat-affected area and extent of precipitate dissolution/reversion. Crack extension being directly related to volume of fine precipitates, J_{1C} of PC welds was less than that of CC welds.

T6 Temper: Size and volume fraction of θ phase was high in T6 temper state than that of T87. Although heat of welding caused partial melting of θ phase and dissolution of strengthening precipitates in HAZ, void nucleation at particle matrix interface was relatively easier in this temper than T87 counterpart. Correspondingly there was reduction in fracture toughness at HAZ of T6 EBW. With PC, fracture toughness further reduced and maintained the same trend as in T87 BM.

4. Conclusions

(1) FZ of electron beam welded AA2219 (7.0 mm thick) consisted of fine-grained microstructure. Sub-grain solidification was cellular and solute segregation was the least. Grain refinement was higher when CC welding was replaced with PC welding.
(2) As-weld strength of T87 base metal was found to be higher than base metal in T6 temper. In the case of T6 base metal, weld ductility was found to be higher. Impact toughness measurements were on par with tensile elongation.
(3) Experimentally determined J_Q values validated J_{1C} criterion for both BM and welds. J_{1C} of BM in T6 temper was found to be double than corresponding T87 temper because of higher volume fraction of strengthening precipitates in the latter.
(4) J_{1C} of FZ was found to be very high (36 kJ/m^2), compared with that of BM-T87 (9 kJ/m^2). Near solution heat treatment, reduced solute partitioning and fine-grained matrix were responsible for such modification. Because of more heat input, cooling rate was lesser in CC welds than PC weld and this was responsible for higher dislocation density in PC weld. Correspondingly, fracture resistant of PC weld was lower than its CC counter part. Comparing to the FZ of T87 BM, absence of dislocations in T6 BM contributed to raise its J_{1C}.
(5) Among the welded samples of both BM tempers, maximum fracture toughness was at the HAZ of T87 BM. CC welds were found to be tougher than PC welds. Precipitate dissolution due to heat of welding and copper depleted zones around grain boundary and second phase appreciably delayed crack propagation at HAZ. Effect of precipitate dissolution and copper depletion was lesser with PC, which brought down its J_{1C} at HAZ. More volume fraction of second phase at HAZ of T6 made ductile tearing easier than identical T87. Hence J_{1C} at HAZ of T6 BM was less than T87 BM.

Acknowledgements

The authors would like to thank Mr. V.M.J. Sharma, Mr. Sudharsan Rao and Mr. Sisupalan, Materials Characterization Lab of Vikram Sarabhai Space Centre for their help.

References

[1] Dudas JH, Collins FR. Preventing weld cracks in high strength aluminium alloys. Weld J 1966;45(6):241s–9s.

[2] Dumolt SD, Laughlin DE, Williams JC. The effect of welding on the microstructure of the age hardenable aluminium alloy 2219. First international aluminium welding conference. Welding research council; 1982. p. 115–33.

[3] Koteswara Roa SR, Reddy GM, Kamaraj M, Prasad Rao K. Grain refinement through arc manipulation techniques in Al–Cu alloy GTA welds. Mater Sci Eng A 2005;404:227–34.

[4] Koteswara Roa SR, Reddy GM, Rao KS, Kamaraj M, Prasad Rao K. Improving mechanical properties of 2219 aluminium alloy GTA welds by scandium addition. Sci Technol Join Weld 2005;10:418–26.

[5] Seshagiri PC, Nair Biju S, Reddy GM, Rao KS, Bhattacharya SS, Prasad Rao K. Improvement of mechanical properties of aluminium–copper alloy (AA2219) GTA welds by Sc addition. Sci Technol Weld Join 2008;12(2):146–58.

[6] Nair Biju S, Phanikumar G, Prasad Rao K, Sinha PP. Improvement of gas tungsten arc and electron beam welded AA2219 (Al–6 wt.%Cu) alloy. Sci Technol Weld Join 2007;12(7):579–85.

[7] Koteswara Roa SR, Reddy GM, Rao KS, Kamaraj M, Prasad Rao K. Reasons for superior mechanical and corrosion properties of 2219 aluminium alloy electron beam welds. Mater Charact 2005;55:345–54.

[8] Galatolo R, Lanciotti A. Fatigue crack propagation in residual stress fields of welded plates.. Int. J Fatigue 1997;19(1):43–9.

[9] Kamp N, Siclair I, Staink MJ. Modeling of fracture toughness in high strength 7xxx aluminium alloys. Mater Sci Forum 2002;396–402:1335–40.

[10] Sharma VMJ, Sree Kumar K, Nageswara Rao B, Pathak SD. Effect of microstructure and strength on the fracture behaviour of AA2219 Al–Cu alloy. International symposium for research scholars on metallurgy. Mat Sci Eng, India; 2008. p. 791–99.

[11] Narayana V, Sharma VMJ, Diwakar V, Sree Kumar K, Prasad BC. Fracture behavior of aluminium alloy 2219–T87 welded plates. Sci Technol Weld Join 2004;9(2):121–30.

[12] Test methods for J_{1C}, a measurement of fracture toughness, E813, Annual Book of ASTM Standards 1996; 03.01: 633–47.

[13] The Metallurgy of Welding, AWS Welding Handbook, 7th ed., vol. 1; 1976. p. 126–8.

[14] Huang C, Kou S. Partially melted zone in aluminium welds–solute segregation and mechanical behavior. Weld J 2001;80:9s–17s.

[15] Bates RC. Correlation of micro void formation, fatigue crack growth rates and facture toughness. In: Proc. Conf on Mechanical Behavior of Materials, Kyoto, Japan; 1974.

[16] G.E. Dieter. Mechanical Metallurgy, SI-metric edition, London: McGraw-Hill Book Company; 1988. p. 256–9.

[17] Rao KS, Reddy GM, Prasad Rao K. Studies on partially melted zones in aluminium–copper alloy welds – effect of techniques and prior thermal temper. Mater Sci Eng A 2005;403:69–76.